frontiers | Frontiers in Chemistry

TYPE Original Research
PUBLISHED 23 September 2024
DOI 10.3389/fchem.2024.1474820

OPEN ACCESS

EDITED BY
Xianglei Kong,
Nankai University, China

REVIEWED BY
Andreas Türler,
University of Bern, Switzerland
Christian Tantardini,
UiT The Arctic University of Norway, Norway
Susanta Lahiri,
Saha Institute of Nuclear Physics (SINP), India

*CORRESPONDENCE
A. Yakushev,
a.yakushev@gsi.de

RECEIVED 02 August 2024
ACCEPTED 06 September 2024
PUBLISHED 23 September 2024

CITATION
Yakushev A, Khuyagbaatar J, Düllmann CE, Block M, Cantemir RA, Cox DM, Dietzel D, Giacoppo F, Hrabar Y, Iliaš M, Jäger E, Krier J, Krupp D, Kurz N, Lens L, Löchner S, Mokry C, Mošať P, Pershina V, Raeder S, Rudolph D, Runke J, Sarmiento LG, Schausten B, Scherer U, Thörle-Pospiech P, Trautmann N, Wegrzecki M and Wieczorek P (2024) Manifestation of relativistic effects in the chemical properties of nihonium and moscovium revealed by gas chromatography studies.
Front. Chem. 12:1474820.
doi: 10.3389/fchem.2024.1474820

Manifestation of relativistic effects in the chemical properties of nihonium and moscovium revealed by gas chromatography studies

A. Yakushev[1,2]*, J. Khuyagbaatar[1,2], Ch. E. Düllmann[1,2,3], M. Block[1,2,3], R. A. Cantemir[1], D. M. Cox[4], D. Dietzel[1,3], F. Giacoppo[1,2], Y. Hrabar[4], M. Iliaš[1,2], E. Jäger[1], J. Krier[1], D. Krupp[5], N. Kurz[1], L. Lens[5], S. Löchner[1], Ch. Mokry[2,3], P. Mošať[1], V. Pershina[1], S. Raeder[1], D. Rudolph[4], J. Runke[1,3], L. G. Sarmiento[4], B. Schausten[1], U. Scherer[5], P. Thörle-Pospiech[2,3], N. Trautmann[3], M. Wegrzecki[6] and P. Wieczorek[1]

[1]GSI Helmholtzzentrum für Schwerionenforschung, Darmstadt, Germany, [2]Helmholtz-Institut Mainz, Mainz, Germany, [3]Department of Chemistry, Johannes Gutenberg-Universität Mainz, Mainz, Germany, [4]Department of Physics, Lund University, Lund, Sweden, [5]Hochschule Mannheim, Mannheim, Germany, [6]Łukasiewicz - Instytut Mikroelektroniki i Fotoniki, Warsaw, Poland

Chemical reactivity of the superheavy elements nihonium (Nh, element 113) and moscovium (Mc, element 115) has been studied by the gas-solid chromatography method using a new combined chromatography and detection setup. The Mc isotope, ^{288}Mc, was produced in the nuclear fusion reaction of ^{48}Ca ions with ^{243}Am targets at the GSI Helmholtzzentrum Darmstadt, Germany. After isolating ^{288}Mc ions in the gas-filled separator TASCA, adsorption of ^{288}Mc and its decay product ^{284}Nh on silicon oxide and gold surfaces was investigated. As a result of this work, the values of the adsorption enthalpy of Nh and Mc on the silicon oxide surface were determined for the first time, $-\Delta H_{ads}^{SiO_2}(\mathrm{Mc}) = 54^{+11}_{-5}$ kJ/mol and $-\Delta H_{ads}^{SiO_2}(\mathrm{Nh}) = 58^{+8}_{-3}$ kJ/mol (68% c.i.). The obtained $-\Delta H_{ads}$ values are in good agreement with results of advanced relativistic calculations. Both elements, Nh and Mc, were shown to interact more weakly with the silicon oxide surface than their lighter homologues Tl and Bi, respectively. However, Nh and Mc turned out to be more reactive than the neighbouring closed-shell and quasi-closed-shell elements copernicium (Cn, element 112) and flerovium (Fl, element 114), respectively. The established trend is explained by the influence of strong relativistic effects on the valence atomic orbitals of these elements.

KEYWORDS

superheavy element chemistry, element 113–nihonium, element 115–moscovium, gas phase chromatography, recoil separators

1 Introduction

1.1 Relativistic effects and periodicity trends in the superheavy element chemistry

Significant progress in the synthesis of the heaviest man-made chemical elements was achieved in the last decades resulting in the completion of the 7th row in the Periodic Table of the Elements (PTE) (Oganessian and Utyonkov, 2015). Due to decreasing nuclear fusion- and survival probabilities with increasing atomic number Z, the production rates of the superheavy elements (SHE) decrease rapidly, reaching a level of a single atom per month for oganesson (Og, element 118) (Oganessian and Utyonkov, 2015). The commonly used technique for SHE isolation is the kinematic separation in a recoil separator. The time between the production of a nuclear fusion reaction product in the target and its implantation as a recoil ion in the detection system is about 1 microsecond, allowing studies of nuclear decay properties of very short-lived isotopes. Experimental methods for chemical studies of SHE are more demanding and time-consuming, and therefore less efficient, especially for short-lived SHE isotopes. This makes studies of chemical properties more challenging (Türler and Pershina, 2013). Among the chemical techniques applied for SHE, a fast and efficient chemical separation can be achieved by gas-solid chromatography studies of volatile species (Türler and Pershina, 2013; Türler et al., 2015).

Chemical properties of yet unstudied SHE can be extrapolated based on the general law of periodicity, which connects the electronic structure of the elements with their position in the PTE. However, with increasing nuclear charge of the SHE, the influence of increasingly important relativistic effects on chemical properties has to be taken into account (Schwerdtfeger et al., 2020; Pyper, 2020; Pershina, 2019; Pershina, 2015). Apparently, the strong contraction of the s and $p_{1/2}$ atomic orbitals (AO) and a large spin-orbit (SO) splitting of the electron shells with the orbital angular momentum quantum number $l \geq 1$, can lead to properties different from those of their lighter homologues. Thus, reliable predictions of chemical properties of SHE become of extreme importance for the heaviest members of groups 12–18 (Schwerdtfeger et al., 2020; Pershina, 2019; Smits et al., 2024). Since the reactivity of atoms is generally connected to the energy level of their valence AO, relativistic calculations of the AO energy levels and of the first ionization potentials (IP) allow assessing the validity of trends within the groups of the PTE (Eliav et al., 2015; Borschevsky et al., 2015; Dzuba and Flambaum, 2016; Trombach et al., 2019). A strong relativistic stabilization of the spherical atomic orbitals with closed-shell $7s^2$ and quasi closed-shell $7p_{1/2}^2$ electronic configurations, together with the large spin-orbit splitting within the 7p shell were shown to result in low AO energies and large IP values for Cn and Fl, respectively (Schwerdtfeger et al., 2020; Pershina, 2015; Eliav et al., 2015). Accordingly, these elements were predicted to be the least reactive members of groups 12 and 14 (Pitzer, 1975; Schwerdtfeger and Seth, 2002). These predictions were recently confirmed experimentally (Eichler et al., 2007; Eichler et al., 2010; Yakushev et al., 2014; Yakushev and Eichler, 2016; Yakushev et al., 2022).

The neighbouring odd-Z elements nihonium (Nh, element 113) and moscovium (Mc, element 115) are presently in the focus of theoretical studies. Since Nh and Mc possess one unpaired electron in the $7p_{1/2}$ or $7p_{3/2}$ subshells, respectively, higher AO energies and lower IP values than for Cn and Fl are predicted for Nh and Mc. This implies that the reactivity of Nh and Mc is higher compared with that of their closed-shell neighbours Cn and Fl. Therefore, chemical reactivity, i.e., the tendency to form chemical bonds, is predicted to be higher for Nh and Mc than for Cn and Fl (Schwerdtfeger et al., 2020; Pershina, 2015; Trombach et al., 2019). However, experimental data on the reactivity of Nh and Mc are required to validate the predicted local minimum at Fl. Indeed, Nh and Mc are expected to form chemical compounds, e.g., hydroxides, which should adsorb more strongly on surfaces than pure atoms (Pershina et al., 2009; Pershina and Iliaš, 2019). Recently, motivated by experimental developments (Yakushev et al., 2021), the interaction of Nh and Mc with Au and quartz surfaces was studied on the basis of periodic relativistic density functional theory (DFT) calculations (Pershina, 2016; Pershina et al., 2021). As a result, equal values of the adsorption energy/enthalpy ($E_{ads} = -\Delta H_{ads}$) on quartz, of 58 kJ/mol, were predicted for elemental Nh and Mc (Pershina et al., 2021). Significantly (by about 100 kJ/mol) higher E_{ads} values were predicted for the adsorption of these elements on the Au (111) surface in several theoretical works (Trombach et al., 2019; Pershina, 2018; Rusakov et al., 2013; Fox-Beyer and van Wüllen, 2012). The obtained E_{ads} values for Nh and Mc turned out to be significantly (by about 50–100 kJ/mol) lower than those of their lighter homologues, Tl and Bi, respectively, on both types of the surfaces, quartz and Au. This is due to the strong relativistic stabilization of the $7p_{1/2}$ AO with respect to the $6p_{1/2}$ AO (Pershina, 2018; Pershina, 2016; Pershina et al., 2021). Thus, all the available predictions agree that both Nh and Mc should be more reactive than Cn and Fl and should easily adsorb at room temperature on Au, and also adsorb on less reactive quartz surfaces (Ilias and Pershina, 2022).

1.2 Experimental challenges and methods

The gas chromatography method has proven being efficient for chemical studies of SHE compared to methods applied for chemical studies in the liquid phase (Türler and Pershina, 2013; Türler et al., 2015). However, the overall efficiency of this method is drastically dependent on the volatility and chemical reactivity of the species under study. In chemistry experiments with the lighter SHE rutherfordium (Rf, element 104) to bohrium (Bh, element 107), the chemical separation was achieved by the combination of the gas-jet transport with gas-solid chromatography (Türler and Pershina, 2013; Türler et al., 2015). A rather low overall efficiency of this multi-step technique was compensated by the relatively high production rates (Türler and Pershina, 2013). A significantly higher overall efficiency was achieved in the chemical study of hassium (Hs, element 108), which was separated in the form of the volatile compound HsO_4 (Düllmann et al., 2002). This technique is based on the combination of gas-solid isothermal chromatography and thermochromatography with a detection system, i.e., by registration of the nuclear decay of a species adsorbed inside the chromatography column itself. The method was developed further during the past two decades, all along to the chemistry studies of the rather inert Cn and Fl (Eichler et al., 2007; Eichler et al., 2010; Yakushev et al., 2014; Yakushev and Eichler, 2016; Yakushev et al., 2022). The necessity of the spatial separation of the single volatile superheavy atoms from other volatile species that contain radionuclides with similar nuclear

decay properties as the nuclide under study and that are created in vastly larger amounts in the form of unwanted side products of the nuclear reactions was recognised (Düllmann et al., 2005). This includes especially Rn isotopes and their daughters. This separation is nowadays routinely achieved by employing physical preseparation in an electromagnetic recoil separator (Yakushev et al., 2014; Yakushev et al., 2022; Wittwer et al., 2010).

Several offline and online studies of the adsorption of Tl species on quartz and gold surfaces were performed, in which a stronger interaction of Tl with Au than with quartz was found (Serov et al., 2013; Steinegger et al., 2016; Lens et al., 2018). In thermochromatography studies under dry and oxygen-free conditions, as well as in the presence of hydrogen, the deposition of Tl on gold was observed at a temperature of about 900°C and was assigned to elemental Tl (Serov et al., 2013). However, independent of the chemical composition in the gas phase, the deposition of Tl on quartz at a temperature of about 300°C was ascribed to be due to TlOH formation caused by a high reactivity of Tl towards hydroxyl groups expected to be present on the quartz surface (Serov et al., 2013). Whereas initial experimental studies with homologues are usually performed in chromatography columns made of bulk materials like quartz (fused silica) or Au metal foils, SHE experiments are often conducted in channels made of silicon radiation detectors with thin hetero-layers covering the detector surfaces. Thin silicon oxide (SiO_2) or Au layers on silicon detectors are produced by oxidation or metal vapour deposition, respectively, and have poorly defined structures. These thin layers serve as reactive solid surface in the gas-solid chromatography process and are usually complex and differ from those used in most theoretical calculations on the adsorption of SHE.

For Cn and Fl, the focus of the chemical studies was on the interaction with Au surfaces (Eichler et al., 2007; Eichler et al., 2010; Yakushev et al., 2014; Yakushev and Eichler, 2016; Yakushev et al., 2022; Wittwer et al., 2010). In these experiments the adsorption enthalpy, $-\Delta H_{ads}^{Au}$, could be measured in a range of approximately 65–35 kJ/mol. Despite the limited number of observed Cn and Fl atoms, both elements were conclusively shown to exhibit high volatility and a rather low reactivity towards Au, characterizing them as volatile metals. In one specific experiment, a SiO_2-covered detector array was installed in front of the Au-covered ones. Neither Fl nor its decay product Cn adsorbed on this SiO_2 surface at room temperature (Yakushev et al., 2022). The low reactivity of Fl, which was confirmed experimentally in several experiments (Eichler et al., 2010; Yakushev et al., 2014; Yakushev and Eichler, 2016; Yakushev et al., 2022), is ascribed to the strong relativistic stabilization of the closed $7p_{1/2}$ subshell (Schwerdtfeger et al., 2020; Pyper, 2020; Pershina, 2019). In contrast to rather inert Cn and Fl, which can be transported as gaseous species to a chromatography and detection setup (Eichler et al., 2010; Yakushev et al., 2014; Yakushev and Eichler, 2016; Yakushev et al., 2022), Nh and Mc might not. This makes experimental studies of these expectedly more reactive elements even more challenging (Yakushev et al., 2021). In fact, the transport of the presumably less volatile Nh to a detection setup was found to be inefficient (likely due to adsorption losses) through a tube made from a material as inert as polytetrafluoroethylene (PTFE) (Yakushev et al., 2021).

The longest-lived known Mc and Nh isotopes can be produced directly or as decay products in nuclear fusion reactions of ^{48}Ca with ^{243}Am and ^{249}Bk targets, leading to the production of Mc and tennessine (Ts, element 117) isotopes, respectively (Oganessian and Utyonkov, 2015). The experimentally easiest access to Mc and Nh is via the nuclear fusion reaction ^{243}Am (^{48}Ca, 3n) ^{288}Mc, which has a high cross section of approximately 10–20 pb (Oganessian et al., 2013; Rudolph et al., 2013; Gates et al., 2015; Oganessian et al., 2022; Oganessian et al., 2022b), similar to that for ^{288}Fl produced in the reaction ^{244}Pu (^{48}Ca, 4n) ^{288}Fl (Düllmann et al., 2010; Såmark-Roth et al., 2023), which was successfully used in chemical studies (Eichler et al., 2010; Yakushev et al., 2014; Yakushev and Eichler, 2016; Yakushev et al., 2022). The decay properties of the members of the ^{288}Mc decay chain are rather well established based on more than two hundred observed decay chains (Oganessian et al., 2013; Rudolph et al., 2013; Gates et al., 2015; Oganessian et al., 2022; Oganessian et al., 2022b). The second member of the ^{288}Mc decay chain, ^{284}Nh, has a half-life of $T_{1/2} = 0.90^{+0.07}_{-0.06}$ s (Oganessian et al., 2022b), similar to those of the isotopes $^{287\text{-}289}$Fl, which were in the focus of recent chemical studies (Yakushev et al., 2021; Eichler, 2013; Dmitriev et al., 2014; Aksenov et al., 2017). However, its directly produced shorter-lived precursor, ^{288}Mc ($T_{1/2} = 193^{+15}_{-13}$ ms) (Oganessian et al., 2022b), was out of reach due to the short lifetime that elapses before the Mc atoms reach the combined chromatography and detection system. The observation of several decay chains originating from ^{284}Nh was claimed in early studies without physical pre-separation (Türler et al., 2015; Eichler, 2013; Dmitriev et al., 2014). The quality of the nuclear decay data in those works was limited by a rather high background in the α-particle spectra (Türler et al., 2015; Eichler, 2013; Dmitriev et al., 2014), which hampered the safe identification of decay chains (Türler et al., 2015; Yakushev et al., 2021). Two recent experiments employing preseparation were conducted behind the Dubna Gas-Filled Recoil Separator (DGFRS) (Akseneov et al., 2017), and behind the TransActinide Separator and Chemistry Apparatus (TASCA) (Yakushev et al., 2021). The low-background conditions led to a much higher sensitivity. However, no conclusive information on the chemical properties of Nh could be derived due to non-observation of ^{284}Nh events in these experiments (Yakushev et al., 2021; Aksenov et al., 2017). The non-observation of Nh atoms in the experiments with preseparation was explained by losses due to the irreversible adsorption of Nh atoms on surfaces they encountered prior to reaching the detection setup, indicating a rather high chemical reactivity of the Nh atoms (Yakushev et al., 2021; Aksenov et al., 2017). Thus, no conclusive and confirmed results on the chemical properties of Nh were obtained in the previous studies. This called for further developments of the experimental setup. Gas chromatography studies of reactive species came within reach by employing the newly developed miniCOMPACT detector array (Yakushev et al., 2021), as demonstrated in adsorption studies of the lighter homologue of Mc, ^{211}Bi[1] and short-lived radioisotopes of the very reactive Fr (Götz et al., 2021). This improved detection system is promising for studies of Nh and is proven to be fast enough to observe a relevant fraction of all produced ^{288}Mc.

1 Dietzel, D., Yakushev, A., Düllmann, Ch. E., Khuyagbaatar, J., Krier, J., Jäger, E., et al. (2024). Off-line single-atom gas chromatographic adsorption studies of ^{211}Bi on SiO_2 surfaces in the novel miniCOMPACT setup. *Submitt. Radiochim. Acta*. [under revision].

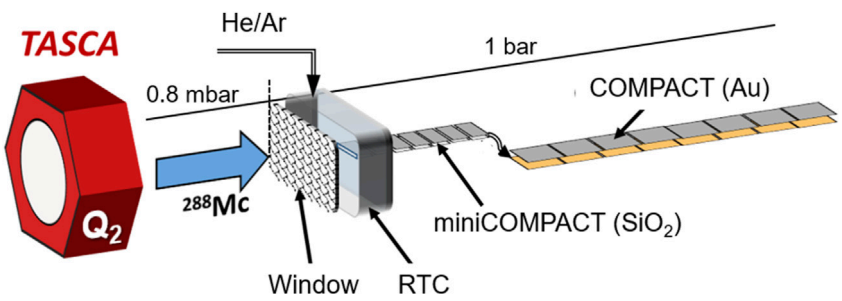

FIGURE 1
Experimental setup behind the second quadrupole (Q_2) at the end of the TASCA separator. Recoiling ^{288}Mc produced in the nuclear reaction were separated with TASCA and entered the Recoil Transfer Chamber (RTC) behind TASCA through a Mylar window. They were thermalized inside the RTC, the inner surface of which was covered with a Teflon™ layer and flushed out with a He/Ar gas mixture to the gas chromatography setup. The first gas chromatography and detection channel, miniCOMPACT, is connected directly to the RTC exit and covered with a SiO_2 layer. The second detector array COMPACT has an Au layer on the detector surface. Both detector arrays were operated at room temperature.

2 Materials and methods

2.1 Experimental setup

The nuclear reaction ^{243}Am (^{48}Ca, 3n)^{288}Mc, utilized for the discovery of element 115, Mc (Oganessian and Utyonkov, 2015), and for the detailed studies of the decay properties of the long α-decay chain starting from the isotope ^{288}Mc (Oganessian et al., 2013; Rudolph et al., 2013; Gates et al., 2015; Oganessian et al., 2022; Oganessian et al., 2022b), was also used for the present chemical studies of Mc and Nh. The gas-filled recoil separator TASCA (Semchenkov et al., 2008) was used to separate products of the fusion-evaporation reaction from the intense primary beam and from the unwanted products of multi-nucleon transfer reactions. The chemical reactivity of Mc and Nh was investigated applying the gas-solid chromatography method in the isothermal regime at room temperature (20°C) (Türler and Pershina, 2013; Türler et al., 2015) via adsorption studies on two surface types, SiO_2 and Au. The gas chromatography setup behind TASCA, as shown in Figure 1, was similar to that described in the first experiment on Nh chemistry at TASCA (Yakushev et al., 2021), except for the connecting tube between the Recoil Transfer Chamber (RTC) and the first detector array. The distance from the RTC gas volume to the first detector element was reduced to about 1 mm.

A pulsed (5 ms beam-on, 15 ms beam-off) $^{48}Ca^{10+}$ ion beam was provided by the UNIversal Linear ACcelerator (UNILAC) at GSI Darmstadt with a typical beam intensity of 5 10^{12} s^{-1}. The target wheel contained four $^{243}Am_2O_3$ targets and rotated with a speed of 2000 revolutions per second, synchronized with beam pulses (Jäger et al., 2014). The ^{243}Am targets with an average thickness of 0.83(1) mg/cm^2 were electro-deposited on 2.2(1) μm Ti foils (Runke et al., 2014). The beam energy in the middle of the ^{243}Am targets was 243.0(2) MeV. In total, 1.2(1) 10^{19} ^{48}Ca ions impinged on the targets during two experimental runs of 15 and 26 days duration, respectively. The evaporation residues were guided through the magnetic recoil separator TASCA with one dipole (D) and two quadrupole (Q) magnets in DQ_1Q_2 configuration, operated in the High-Transmission Mode (Semchenkov et al., 2008). TASCA was filled with He at a pressure of p_{He} = 0.8 mbar and was set to a magnetic rigidity of $B{\cdot}\rho$ = 2.21 Tm (Rudolph et al., 2013; Khuyagbaatar et al., 2012) to center ^{288}Mc recoils in the TASCA focal plane. The nominal transmission efficiency in TASCA to focus the recoiling ^{288}Mc ions into the RTC window area is about 40% (Yakushev et al., 2021). Products recoiling from the target and separated in TASCA according to their magnetic rigidities were thermalized in the RTC in a 1:1 gas mixture of He and Ar at 1 bar, similarly to the first Nh study at TASCA (Yakushev et al., 2021). Due to a large number of collisions with gas atoms, the isolated ions lose their kinetic energy, and their charge state is decreased accordingly to +1 or +2. The thermalized ions can be neutralized in gas by recombination or collisions with gas impurities or with any surface. The gas was circulated in a closed loop by a membrane pump at a flow rate of 2.9 L/min. The rare gases, He (99.9999%) and Ar (99.999%), were purified further by passing cartridges MC50-902FV and MC400-902FV (SAES™). These cartridges had internal particle filters, which efficiently remove aerosol particles with sizes down to 3 nm diameter and reduced the water and oxygen content to a level of about 1 ppm. The most critical impurity, water, was monitored by the dew point transmitter Pura (Michell Instruments). The isolated nuclear reaction products were flushed into the gas chromatography and detection setup. Two different detector channels were used, namely, a miniCOMPACT detector (Yakushev et al., 2021; Götz et al., 2021), followed by a COMPACT detector, used in the previous Fl chemistry studies at TASCA (Yakushev et al., 2014; Yakushev et al., 2022). The miniCOMPACT detector array was directly connected to the RTC via an exit slit with a cross section of (10.0 × 0.5) mm^2, fitting to the cross section of the miniCOMPACT channel, and allowing for an effective transport and detection of less-volatile species. As Nh and Mc should interact more strongly with gold than with quartz (Pershina et al., 2021), the silicon photodiodes of the miniCOMPACT detector array were covered with a 30–50 nm-thick SiO_2 layer. The photodiodes of the COMPACT detector array were covered with a 30 to 50 nm-thick Au layer. A 30-cm long capillary made of PTFE with an inner diameter of 2 mm connected the Au-covered COMPACT detector array to the miniCOMPACT array. Both detectors consisted of two panels, each divided into 32 detector elements. The opposite detector panels (top and bottom) were mounted with the active detector surfaces facing each other, and thus, forming a narrow gas channel with a distance between the opposite panels of 0.6 mm or 0.8 mm for the COMPACT array and the miniCOMPACT array, respectively. Each detector panel of the miniCOMPACT and COMPACT detectors consists of 32 Positive-Intrinsic-Negative (PIN) diodes mounted in a row (Wegrzecki et al., 2013). They registered α particles and fission

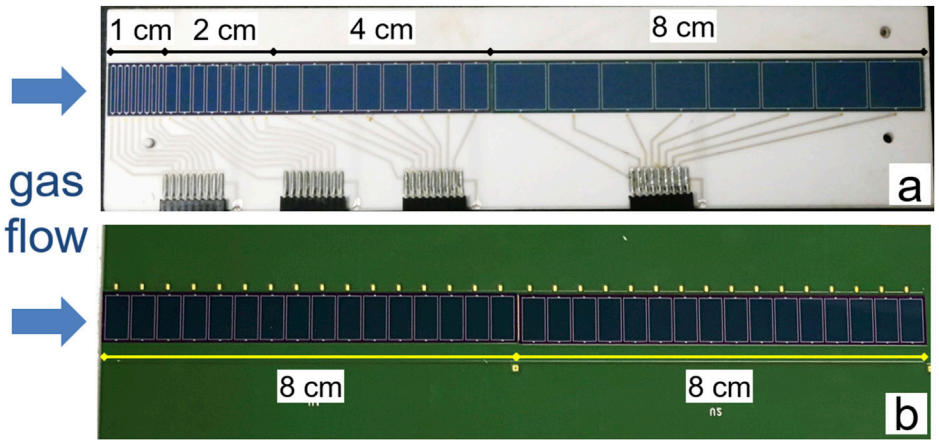

FIGURE 2
The open miniCOMPACT detector arrays. Only one of two detector panels forming the narrow channel is shown, as used in the first **(A)** and second experimental run **(B)**. The direction of the gas flow through the detector channel is indicated with arrows.

fragments emitted by nuclear decays occurring inside the detector channel. Two different segmentation geometries of the miniCOMPACT detector arrays were used in the first and the second run. In the first run, a 15-cm long miniCOMPACT array had differently-sized detector elements mounted on a ceramic printed circuit board (PCB) as shown in Figure 2A. Each detector panel consisted of two silicon chips, which were 7 cm and 8 cm long. The first 7-cm long silicon chip was divided into three eight-element groups. They were 1, 2, and 4 cm long. The following 8-cm long chip had eight equal detector elements. In the second run, a 16-cm long miniCOMPACT detector array was used. The panels of the second detector consisted of two equal, 8-cm long silicon chips, each divided into sixteen detector elements, and were mounted on a multilayer FR4 PCB (flame retarding printed circuit board) as shown in Figure 2B.

2.2 Method of calculation

Theoretical calculations accompany our experimental study. We have calculated electronic energies of gas-phase reactions that single metal atoms (M, where M = Bi and Mc) and singly-charged metal ions (M+) could undergo in the recoil chamber. The aim was to investigate a potential reactivity of Bi and Mc species towards water and oxygen, which are present as gas impurities at the trace level.

Our considered systems are SHE, which can only be treated appropriately when relativistic effects are explicitly taken into account in the calculations. A well-proven method for such work is the Density Functional Theory (DFT) approach (Hohenberg and Kohn, 1964). The theory underlying is the DFT is the self-consistent Kohn–Sham approach (Kohn and Sham, 1965). Kohn-Sham DFT is a first-principles computational method to predict accurately chemical properties and to analyse them in simple chemical terms. Specifically, the Kohn-Sham approach in general delivers correct electron densities and related properties, as well as the total energy, but implies a one-electron representation of the many-electron systems. Although the precise exchange-correlation (XC) functional is unknown, by using appropriate XC functionals, binding energies may typically be determined with a precision of a few kJ/mol (Te Velde et al., 2001). DFT keeps at all levels of approximation the appealing one-electron molecular orbital (MO) view on chemical reactions and properties. The computed orbitals are suitable for typical MO-theoretical analyses and interpretations. The Kohn-Sham method also effectively incorporates all correlation effects. The calculations of electronic structures of the molecules of interest were performed using the Density Functional Theory approach implemented in the AMS ADF software (SCM, 2024). The AMS electronic structure approach uses the zeroth order regular approximation (ZORA) two-component Hamiltonian incorporating both scalar relativistic (SR) and SO relativistic effects. Although the regular approximation is not gauge invariant at any order, the scaled ZORA energy is exactly gauge invariant for hydrogen ions. The scaled ZORA approach, as it was used in our ADF calculations, is nearly gauge-invariant for many-electron systems, as explained in detail in Ref. (Van Lenthe et al., 1994). Briefly, the scaled ZORA equation differs from the original ZORA equation by the denominator to introduce a scaling of the ZORA energy. The calculated scaled-ZORA total energies prove to be very close to the fully relativistic energies for atoms. For all-electron calculations, the original ZORA total energy cannot be used as it suffers from gauge invariance problems that are particularly serious for deep-core states. The scaled ZORA total energy solved this problem, delivering results within “chemical” accuracy. The same holds for two-component calculations with the SO ZORA Hamiltonian. The spin-polarized non-collinear approach, also called as Kramers unrestricted approach, was applied. The basis sets are a combination of numerical AOs and Slater-type orbitals (STOs). The used basis sets are of the Triple Zeta plus Double Polarization (TZ2P) size. These basis sets are well saturated and describe the polarization of the electron density of an atom in molecules. Since correlation effects are also very important for SHE systems and can contribute up to the 50% of the binding energy, those are taken into account by using XC functionals. We utilized the BP86 (Becke, 1988) exchange-correlation functional. The geometry optimizations of studied molecules were carried out with the SO ZORA Hamiltonian, ensuring that both SR and SO relativistic effects were reflected in the optimized molecular structures.

TABLE 1 Energies of α particles ($E_α$) and SF (E_{SF}) fragments[a] and time intervals (Δt) of the observed decay chain members and fission events without α-decaying precursors. The total time difference for decay chain members following missing ones are given in parentheses.

Chain number	^{288}Mc $E_α$, MeV	^{284}Nh $E_α$, MeV $Δt_1$, s	^{280}Rg $E_α$, MeV $Δt_2$, s	^{276}Mt $E_α$, MeV $Δt_3$, s	^{272}Bh $E_α$, MeV $Δt_4$, s	^{268}Db $E_{α/SF}$, MeV $Δt_5$, h	^{264}Lr E_{SF}, MeV $Δt_6$, h
1	**10.33**[b] –	**9.84**[c] 0.646	missing	**9.51** (22.86)	missing	**85 + n.d.**[d] (40.6)	
2	**10.22** –	missing	**9.32** (1.48)	missing	**8.98** (2.06)	**7.83** 9.5	**74 + 70** 4.7
3	missing	**9.25** –	**9.71** 3.33	9.76 0.515	**9.05** 7.43	**>64+>66**[e] 13.8	
4	missing	**9.79** –	9.70 9.22	**8.95** 0.289	**8.97** 3.27	**7.69** 24.2	98 + 110 6.4
5	missing	**9.88** –	**9.64** 3.69	9.51 0.938	**8.95** 50.13	93 + 116 43.4	
6	missing	**9.57** –	**9.69** 3.19	**9.56** 0.813	**8.91** 8.94	**112 + n.d**[d] 64.8	
7	missing	**9.47** –	**9.70** 0.813	**0.76**[f] 0.125	missing	**7.77** (14.3)	**117 + 66** 13.3
8	missing	**9.85** –	**9.04** 3.05	**9.59** 0.105	**9.04** 34.84	**7.82** 7.8	**49 + n.d** 12.9
9	missing	**9.86** –	9.53 0.253	**9.27** 0.125	**8.82** 8.39	**91 + 93**[g] 19.1	
10	**10.38** –	**9.44** 0.318	9.84 19.38	**9.47** 2.05	missing	n.d.[h]	
11	missing	**9.98** –	**9.72** 8.41	**9.45** 0.285	missing	n.d.[h]	
12	10.02 –	**9.84** 1.69	**9.72** 0.293	missing	**9.05** (3.93)	**116 + 86**[g] 37	
13	missing	9.92 –	**9.78** 1.93	**9.54** 0.084	8.07 5.76	**111 + 83**[g] 81.2	
14	missing	9.96 –	missing	**9.62** (92.68)	8.58 13.46	**83 + 89**[g] 30.1	
15	missing	**9.60** –	**9.68** 0.937	**9.44** 1.12	**9.06** 5.18	70 + 75[i] 8.9	
16	missing	**9.65** –	**9.61** 6.74	**9.24** 0.034	**8.84** 6.42	**87 + 103**[i] 43.7	
17	missing	**9.63** –	**9.58** 16.91	**9.37** 0.432	missing	**11 + 28**[i] 21.9	
18	missing	**9.75**	missing	**9.63** (0.551)	**9.08** 5.44	77 + n.d.[i,j] 31.8	

Fission events without α-decaying precursors				
SF 1	SF 2	SF 3	SF 4	SF 5
105 + n.d	104 + 113	91 + 70	99 + 93	99 + 22

[a]The SF fragment energy values were not corrected for the pulse height defect.

[b]The energy values of decay chain members, where decay occurred during the beam-off periods, are given in bold.

[c]The decays from decay chain members starting with ^{284}Nh occurred 4 mm downstream to the decay from ^{288}Mc.

[d]One SF fragment was not detected (n.d.) due to the not working opposite detector strip.

[e]This event occurred in the second Au-covered COMPACT detector. The full SF fragment energy could not be detected due to a high amplification gain of the preamps.

[f]A small energy signal was detected. This can be explained by α particle hitting mainly the inactive area of the detector.

[g]No candidates for α decay of ^{268}Db.

[h]SF events were not detected due to a technical problem with the data acquisition system lasted for several hours.

[i]Several candidates for the α decay were found. No unambiguous conclusion on α decay of ^{268}Db could be made.

[j]All signals were registered on the same detector side pointing at the deposition on the inactive surface of the opposite detector side.

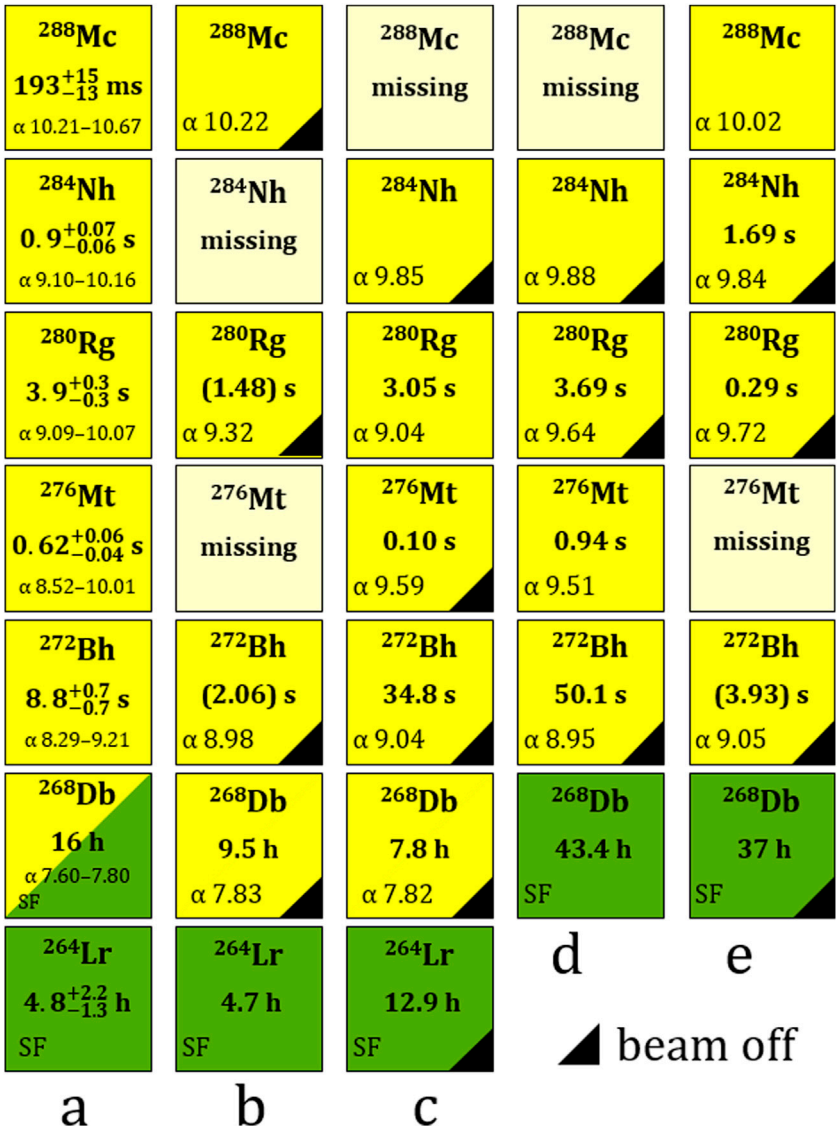

FIGURE 3
The decay properties of the ^{288}Mc-decay chain members. **(A)** The presently known decay properties along the long decay chain from ^{288}Mc are shown for comparison (Oganessian et al., 2022). **(B–E)** Four representative decay chains (#2, #8, #5, #12 in Table 1) out of eighteen observed in our experiments are shown. Color coding: α decay (yellow) and spontaneous fission (green). Half-lives **(A)** and correlation times **(B–E)** are indicated for decay chain members. The total time difference for decay chain members following missing ones are given in parentheses. The α-particle energies are given in mega electron volts (MeV). The black triangles represent the decays observed during beam-off periods.

3 Results

3.1 Observation of decay chains from ^{288}Mc and ^{284}Nh

A search for position- and time-correlated nuclear decay chains was performed, to identify multiple genetically-linked members of the well-known long ^{288}Mc decay chain, decaying by emission of α-particles within the energy interval (8.0–10.5) MeV and within a 200-s time interval. This search resulted in the finding of eighteen decay chains, seven in the first run and eleven in the second run. The decay chains were assigned to ^{288}Mc or to ^{284}Nh in accordance with their known decay properties (Oganessian et al., 2022; Oganessian et al., 2022b; Forsberg et al., 2016; Rudolph, 2022). As usual for such an experiment, where an atom is adsorbed on a detector surface inside a gas chromatography channel, α particles or fission fragments have to penetrate several inactive layers. They deposit a fraction of their kinetic energy in a SiO_2 or Au layer on top of the detector surface, and then in an inactive silicon layer on top of the diode. In addition, if the particles cross the detector channel, they experience further energy loss in the gas. These energy losses depend strongly on the angle to the surface, at which the particle is emitted. Thus, the energy distributions of registered α particles and spontaneous fission (SF) fragments have usually tailing towards low energies in contrast to the orresponding energy distributions registered in physics experiments, where the ions are implanted into

a silicon detector. The energy calibration of the detectors was performed using a ^{227}Ac source emanating ^{219}Rn, and was linearly extrapolated up to the fission fragment energies. Independently, the search for high-energy events with an energy of $E_{SF} > 20$ MeV was performed on a time scale of hours to days, to identify candidates for long-lived decay chain members terminating the decay chains by SF. In total, twenty-one candidate SF events were identified in the two runs. Sixteen SF events, twelve with two fragments and four with one fragment, occurred at the same detector positions, where chains with multiple α-decaying members were also detected, several hours before the SF events. These position-correlated SF events were assigned to the SF decay of ^{268}Db or ^{264}Lr (Oganessian et al., 2022). For two out of the eighteen registered decay chains, no terminating SF events were found, presumably due to a several-hour long problem with the data acquisition system in the period following the detection of these two chains. The decay parameters, energies and time intervals of the members of all observed decay chains are listed in Table 1. Figure 3 shows four representative examples (b–e) of observed chains, along with the reference decay chain (a).

Based on the decay properties along the long ^{288}Mc decay chain (Figure 3A), four out of eighteen chains were attributed to originate from ^{288}Mc (*cf.* Table 1). The missing observation of ^{288}Mc in the other fourteen chains is attributed to the decay losses of the short-lived nucleus ^{288}Mc ($T_{1/2} = 193^{+15}_{-13}$ ms) during the transport of the ^{288}Mc atoms into the detector channel. The observed ratio of the number of detected decay chains starting with ^{288}Mc decay to that of chains starting with ^{284}Nh ($T_{1/2} = 0.90^{+0.07}_{-0.06}$ s) allows a rough estimate of the mean flush-out time from the RTC window into miniCOMPACT of about 0.4 s. The transport time corresponds to approximately two half-lives for ^{288}Mc, but it was short enough for the efficient transport of ^{284}Nh. Within the observed decay chains, eleven α particles from the decay chain members ^{284}Nh, ^{280}Rg, ^{276}Mt, ^{270}Bh, were missing, in agreement with the mean detection efficiency for a single α particle emitted inside the miniCOMPACT detector channel of about 80%. The search for the α decay of the long-lived ^{268}Db was performed within the energy interval (7.7–8.0) MeV and within the time interval between the last member of the α-decay chain occurring during the time interval of 200 s and the concluding SF event. Several candidates for α decay of ^{268}Db were found (Table 1). However, this search was hindered in some cases by a non-zero background in this energy range, especially from non-volatile byproducts within the first centimeters of the miniCOMPACT detector. The measured time intervals between neighbouring members of all registered decay chains show a very good agreement with the known half-lives, deduced from the observation of about two hundred chains in physics experiments (Oganessian et al., 2013; Rudolph et al., 2013; Gates et al., 2015; Oganessian et al., 2022b). The experimental distributions of correlation times for the decay chain members ^{284}Nh, ^{280}Rg, ^{276}Mt, ^{272}Bh and ^{268}Db are shown in Figure 4, in comparison with lifetime probability curves calculated for the recently published most precise half-lives (Oganessian et al., 2022; Oganessian et al., 2022b).

Five SF events, which were observed without position and time correlation to any α-decaying precursors within the energy range (9.0–10.5) MeV and a time interval of 1000 s. They could not be assigned to any registered long decay chain from ^{288}Mc or

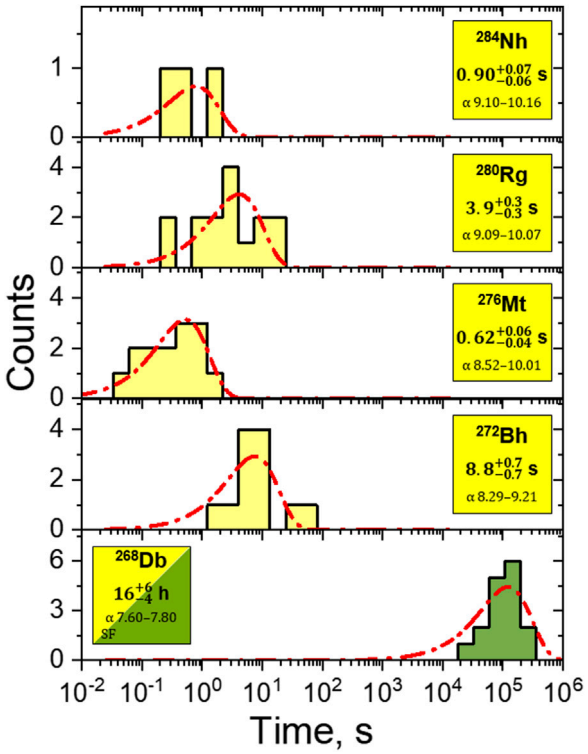

FIGURE 4
The lifetime distributions of the observed decay chain members ^{284}Nh, ^{280}Rg, ^{276}Mt, ^{272}Bh, and ^{268}Db. The experimental lifetime distributions are shown for ^{284}Nh, ^{280}Rg, ^{276}Mt, ^{272}Bh, and ^{268}Db (bars), in comparison with the lifetime probability curves (dash-dotted lines) calculated for the recently published half-lives of these isotopes (Oganessian et al., 2022; Oganessian et al., 2022b). Yellow denotes α-decay, green denotes spontaneous fission.

^{284}Nh. Two such SF events were registered in the first centimeter of the miniCOMPACT array, and three at the 4th, 6th and 10th centimeter. In four cases, both fission fragments were detected. These SF-only events were considered as real ones and could be attributed to SF branches in early chain members (Oganessian et al., 2022; Forsberg et al., 2016; Rudolph, 2022). A detailed analysis on decay scenario aspects along the decay chain from ^{288}Mc will be published elsewhere[2]. Even though the spatial distribution of these SF events in the detector channel resembles the distribution of decay chains from ^{284}Nh, the ambiguity in the assignment of these SF-only events did not allow including them for the evaluation of the chemical behaviour.

A comparison of the number of events registered in the present experiment to the number of decay chains from the Mc decay spectroscopy experiment at TASCA (Rudolph et al., 2013) normalized to the number of produced ^{288}Mc nuclei reveals that roughly 40% of the reaction products guided to the TASCA focal plane were extracted into the gas chromatography channel. The losses were primarily caused by adsorption of non-volatile species on the RTC surface before reaching the detection setup. In addition,

2 Khuyagbaatar, J., Yakushev, A., Düllmann, Ch. E., and Mošať, P. (2024).

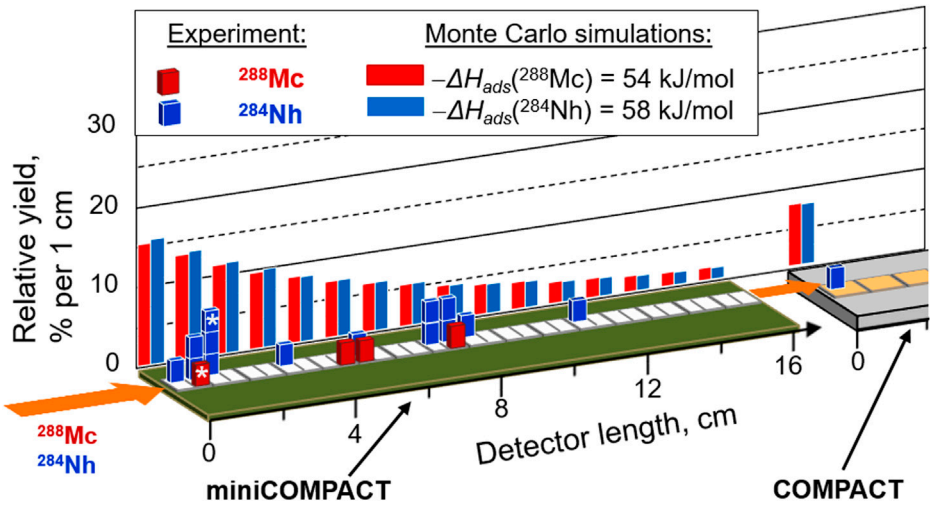

FIGURE 5
Event distribution in the detection setup. The positions of all observed decay chains in the detection setup assigned to ^{288}Mc (red bars) and ^{284}Nh (blue bars) are shown together with results of Monte Carlo simulations for the most probable values of the adsorption enthalpy on SiO_2, $-\Delta H_{ads}$ (Mc) = 54 kJ/mol and $-\Delta H_{ads}$ (Nh) = 58 kJ/mol, for Mc and Nh, respectively. According to simulations, a fraction of about 8% of both, Mc and Nh atoms, entering the miniCOMPACT pass through. This fraction is indicated as deposition in the first centimeter of COMPACT. In one decay chain, the observed decays from ^{288}Mc and ^{284}Nh were distributed over two detectors; their positions are marked with an asterisk.

decay losses also significantly contributed to the overall losses of the short-lived ^{288}Mc.

3.2 Distribution of Mc and Nh in the detection setup

All observed decay chains originating from ^{288}Mc or ^{284}Nh were found in the miniCOMPACT detector, except for one decay chain from ^{284}Nh, which was registered in the first centimeter of the Au-covered COMPACT. Thus, while all four Mc atoms adsorbed on the SiO_2 surface, one of the 14 Nh atoms passed the miniCOMPACT detector and a 30-cm long connecting tube made of PTFE between miniCOMPACT and COMPACT, but adsorbed on the very first Au-covered detector. This observation may suggest a stronger interaction with the Au surface compared to interaction with SiO_2 and PTFE surfaces, in line with the predictions (Pershina et al., 2021). This encourages future studies with higher statistics. The positions of the observed decay chains starting with ^{288}Mc and starting with ^{284}Nh in the detector channel are presented in Figure 5. All four events originating from ^{288}Mc and about 85% of the ^{284}Nh events were registered in the first half of the SiO_2-covered miniCOMPACT detector.

4 Discussion

Atoms without retention on the surface would pass miniCOMPACT within about 20 ms. Thus, almost all Nh and Mc nuclei would pass the miniCOMPACT detector array without decay. Clearly, the observation of the decay of Nh and Mc nuclei in the miniCOMPACT detector array demonstrated retention due to adsorption of Nh and Mc on SiO_2 at room temperature. A key question is in which chemical form Mc and Nh deposited on the SiO_2 detector surface. Despite the short lifetime of Mc and Nh, the possibility to form compounds through rare interactions with gas impurities cannot be excluded. The main gas impurities, O_2 and H_2O,

TABLE 2 Calculated values of the energy of reaction for selected chemical reactions of metal M (M = Bi, Mc) with oxygen and water. The initial metallic species are neutral atoms (M) or monovalent cations (M(+)). The initial oxygen and water are molecular O_2 and H_2O.

Chemical reaction	Energy of reaction, eV			
	M = Tl	M = Bi	M = Nh	M = Mc
$M(+) + O_2 = MO(+) + O$	5.928	2.666	5.705	5.697
$M(+) + H_2O = MO(+) + H_2$	5.431	2.168	5.207	5.200
$M(+) + H_2O = M(OH) + H (+)$	9.448	8.613	9.547	10.200
$M + O_2 = MO(+) + O (-)$	10.977	8.928	11.765	10.320
$M + H_2O = M(OH) + H$	2.065	2.444	5.073	2.393

were kept at a ppm level at most, similarly to the previous experiments at TASCA (Yakushev et al., 2014; Yakushev et al., 2022). To form compounds (oxides or hydroxides) in reactions with traces of O_2 and H_2O, Mc ions or atoms should be able to break rather strong chemical bonds in the O_2 and H_2O molecules after their thermalization in the gas. Energies of selected reactions of the M atoms and M+ ions with the O_2 and H_2O molecules, where M is a superheavy element Mc or Nh, or their nearest homologues Bi or Tl, were calculated with the ADF BAND code and are presented in Table 2. All values are positive, ranging from 2.07 to 11.77 eV. Because of the rather high positive values of the heat of reaction, these interactions are not energetically favored at room temperature for Mc and Nh and neither for their homologues Bi and Tl. Thus, the thermodynamical analysis of possible reactions with trace gas impurities clearly suggests that Mc and Nh should stay in the elemental form before they adsorb on the SiO_2 surface. In order to obtain more quantitative information on the interaction strength between Mc and Nh atoms and the SiO_2 surface, the Monte Carlo simulation method was applied to obtain numerical information on the interaction strength between SHE species and a surface. This approach is based on the model of mobile adsorption (Zvara, 1985) and allows to simulate individual histories of a large number of single atoms (e.g., 10^6) migrating through the chromatography column, using actual experimental parameters including the dimension of the column, the gas composition and flow rate, the radionuclide's half-life etc. Single Mc or Nh atoms moving with the carrier gas along the detector arrays experience many collisions with the surface. In each surface collision, the adsorbed atom is immobilized at the surface for a time τa, which depends on the (experimentally known) oscillation period τ_0, the activation energy needed for its desorption from the surface (E_{des}), which is a free parameter, and on the temperature, according to the Frenkel's equation (Frenkel, 1948) (Equation 1).

$$\tau_a = \tau_0 \cdot exp\left(\left(\frac{E_{des}}{RT}\right)\right) \quad (1)$$

Supposed that the energy needed for the desorption is equal to the negative adsorption enthalpy, $E_{des} = -\Delta H_{ads}^{SiO_2}$, such simulations were performed for the adsorption of Mc and Nh atoms on SiO_2 resulting in simulated distributions of Mc and Nh for different $-\Delta H_{ads}^{SiO_2}$ values. The statistically analysed agreement between the experimental distributions of ^{288}Mc and ^{284}Nh in miniCOMPACT and the simulated ones enabled deducing the adsorption enthalpy values of Mc and Nh atoms on the SiO_2 surface, ($-\Delta H_{ads}^{SiO_2}$), to 54 $^{+11}_{-5}$ kJ/mol for Mc and 58 $^{+8}_{-3}$ kJ/mol for Nh. The distribution of Mc and Nh atoms in miniCOMPACT for their most probable $-\Delta H_{ads}^{SiO_2}$ values are depicted in Figure 3. The lower and upper limits for these values were determined for a confidence interval (c.i.) of 68% by statistical analysis employing a method of c.i. calculation for experiments with small event numbers (Brüchle, 2003). The obtained $-\Delta H_{ads}$ values for Mc and Nh on the SiO_2 surface agree with the theoretically predicted E_{ads} values for elemental Nh and Mc on quartz (Pershina et al., 2021), supporting the assignment of Mc and Nh deposition in elemental form.

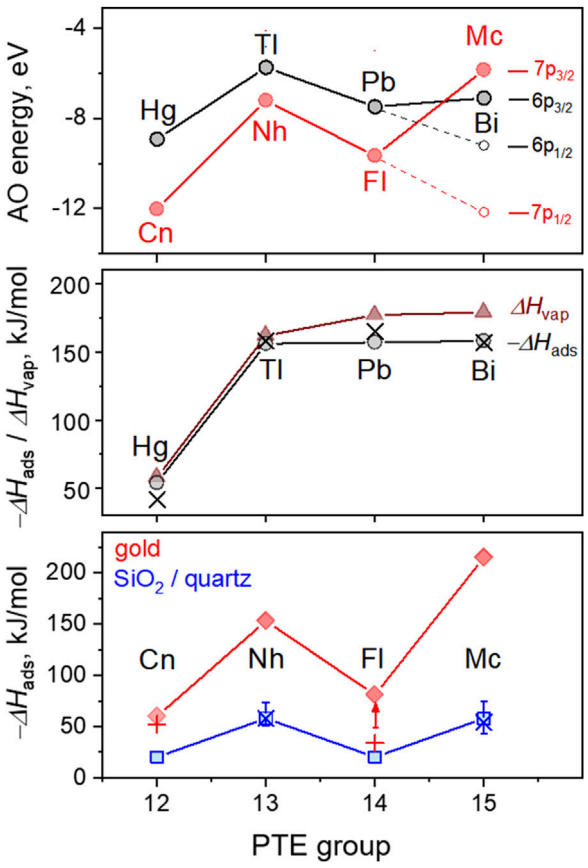

FIGURE 6
Calculated energies of the highest occupied atomic orbitals for elements of the groups 12–15 of the 6th and 7th period; adsorption enthalpies ($-\Delta H_{ads}$) on quartz (theoretical values of 6p and 7p elements and experimental values of 6p elements); $-\Delta H_{ads}$ values on the SiO_2 (experimental values of 7p elements) and Au surfaces (theoretical and experimental values of 7p elements); and vaporization enthalpies (ΔH_{vap}). Upper panel: calculated Dirac-Fock energies of the highest occupied AO (in eV) are shown with red symbols for Cn to Mc and with black ones for their homologues, Hg to Bi (Desclaux, 1973). The black and red arrows show the values of the spin-orbit splitting for the 6p and 7p shells, respectively. Middle panel: The calculated and experimental values of $-\Delta H_{ads}$ on quartz for SHE homologues, Hg to Bi, are shown as grey circles and black crosses, respectively (Pershina, 2018; Trombach et al., 2019; Serov et al., 2013; Steinegger et al., 2016; Düllmann et al., 2022; Kraus, 2021). The experimental values of ΔH_{vap} are shown as brown solid triangles (Zhang et al., 2011). Lower panel: calculated values of $-\Delta H_{ads}$ on quartz and Au for Cn to Mc are shown with blue square and red diamond symbols, respectively (Pershina, 2018; Pershina et al., 2021; Trombach et al., 2019; Düllmann et al., 2022). Experimental $-\Delta H_{ads}$ on Au for Cn and Fl are shown as red crosses and an arrow in the case of a limit (Eichler et al., 2010; Yakushev et al., 2014; Yakushev et al., 2022). Experimental values from this work, $-\Delta H_{ads}^{SiO_2}$ (Mc) = 54 $^{+11}_{-5}$ kJ/mol and $-\Delta H_{ads}^{SiO_2}$ (Nh) = 58 $^{+8}_{-3}$ kJ/mol, are shown by blue crosses with error bars. All panels: the lines connecting the data points are shown to guide the eye. All $-\Delta H_{ads}$ values are given in kJ/mol.

Theoretical and experimental thermodynamic values for the reactivity and volatility of the superheavy elements in groups 12–15 and their nearest lighter homologues are summarized in Figure 6. For the heaviest members of the groups 12–15 of the PTE, trends in AO energies of the highest occupied orbitals show an irregular course with minima for groups 12 and 14. The spread is

significantly more pronounced for SHE compared with their lighter homologues due to the strong spin-orbit splitting in the 7p shell and stabilisation of the 7s and $7p_{1/2}$ (sub) shells in Cn and Fl, respectively (Figure 6, upper panel). This trend also determines the chemical behaviour, e.g., the adsorption strength of these elements on the gold and quartz surfaces. The calculated and experimental values of $-\Delta H_{ads}$ on quartz for elements of the 6th row are shown in Figure 6 (middle panel) in comparison with their heat of vaporization (ΔH_{vap}) values.

The trend in $-\Delta H_{ads}$ values for the 6p elements is indicative of a strong increase in the interaction strength with the surface from Hg to Tl that remains almost unchanged for Tl, Pb, and Bi (Pershina, 2018; Trombach et al., 2019; Düllmann et al., 2022). The theoretical $-\Delta H_{ads}$ values show a good agreement with the experimental ones (Serov et al., 2013; Steinegger et al., 2016; Kraus, 2021). The experimental $-\Delta H_{ads}$ value for Bi was obtained in recent off-line gas chromatography studies with Po and At isotopes at the U-120 M cyclotron in Řež, Czech Republic, and will be published elsewhere. The ΔH_{vap} values for these elements follow a similar trend (Zhang et al., 2011). For the heaviest members of groups 12–15, the calculated and experimental $-\Delta H_{ads}$ values on quartz and Au are shown in Figure 6 (lower panel). The predicted $-\Delta H_{ads}$ values for adsorption of Nh and Mc on quartz are significantly lower than those of their lighter homologues, Tl and Bi, respectively. Moreover, the trend of the $-\Delta H_{ads}$ values of the superheavy elements Cn to Mc has also an irregular course, similar to that of the energies of their highest occupied AOs. This difference in the trends between the 6p and 7p elements is attributed to the larger spin-orbital effects on the 7p AO (Figure 6, upper panel) and the relativistic stabilization of the $7p_{1/2}$ orbital, and is in line with the reduced chemical reactivity in Fl (Schwerdtfeger et al., 2020; Pershina, 2015; Eliav et al., 2015).

5 Conclusion

Eighteen decay chains originating from ^{288}Mc and its decay products were identified upon adsorption on silicon oxide and gold surfaces (Table 1). The decay properties of the registered chain members are in excellent agreement with those obtained in earlier physics studies. Taking into account experimental conditions and results of state-of-the-art theoretical predictions, we conclude that Nh and Mc were deposited on the silicon oxide surface in the elemental state. The thermodynamic quantities for Nh and Mc, namely, $-\Delta H_{ads}^{SiO_2}(\mathrm{Mc}) = 54^{+11}_{-5}$ kJ/mol and $-\Delta H_{ads}^{SiO_2}(\mathrm{Nh}) = 58^{+8}_{-3}$ kJ/mol (68% c.i.), were deduced by using Monte Carlo simulations. Our experimental observations indicate a stronger chemical interaction of Nh and Mc compared to their neighbours Cn and Fl, in accordance with theoretical predictions. The obtained values are significantly (about 100 kJ/mol) lower than those of their lighter homologues, Tl (Serov et al., 2013; Steinegger et al., 2016) and Bi. Thus, the lowest chemical reactivity in groups 13 and 15 is observed for the 7p elements Nh and Mc. This is due to strong relativistic effects, i.e., the large energy splitting in the 7p shell and the stabilization of the $7p_{1/2}^2$ subshell has been confirmed experimentally. This work opens the door to future chemical research with even heavier elements, Lv and Ts, to shed light on the evolution of relativistic effects as the $7p_{3/2}$ subshell is being filled. However, a fast and efficient extraction from a gas-filled chamber to a chemistry setup is required for future SHE experiments beyond Mc to minimize the transport time of very short-lived products to a chemistry apparatus down to a few milliseconds. Recent numerical and experimental results show promise for such chemistry experiments, if a chemistry setup is coupled to a buffer gas cell, in which ions are carried to a chemistry device by electrical fields (Varentsov and Yakushev, 2019; Götz et al., 2021).

Data availability statement

The raw data supporting the conclusions of this article will be made available by the authors, without undue reservation.

Author contributions

AY: Conceptualization, Data curation, Formal Analysis, Investigation, Methodology, Project administration, Validation, Writing–original draft, Writing–review and editing. JKh: Data curation, Formal Analysis, Investigation, Software, Validation, Writing–review and editing. CD: Conceptualization, Funding acquisition, Methodology, Project administration, Resources, Supervision, Validation, Writing–review and editing. MB: Formal Analysis, Investigation, Validation, Writing–review and editing. RC: Data curation, Methodology, Resources, Software, Writing–review and editing. DC: Data curation, Formal Analysis, Investigation, Writing–review and editing. DD: Data curation, Formal Analysis, Investigation, Validation, Writing–review and editing. FG: Data curation, Investigation, Validation, Writing–review and editing. YH: Data curation, Formal Analysis, Writing–review and editing. MI: Methodology, Software, Validation, Writing–review and editing. EJ: Data curation, Resources, Software, Writing–review and editing. JKr: Data curation, Methodology, Resources, Writing–review and editing. DK: Data curation, Formal Analysis, Methodology, Writing–review and editing. NK: Data curation, Formal Analysis, Methodology, Resources, Software, Validation, Writing–review and editing. LL: Methodology, Writing–review and editing, Conceptualization, Data curation, Formal Analysis, Investigation. SL: Data curation, Formal Analysis, Resources, Software, Writing–review and editing. CM: Data curation, Methodology, Writing–review and editing. PM: Data curation, Formal Analysis, Investigation, Methodology, Software, Validation, Writing–review and editing. VP: Conceptualization, Formal Analysis, Investigation, Software, Validation, Writing–review and editing. SR: Data curation, Formal Analysis, Validation, Writing–review and editing. DR: Data curation, Formal Analysis, Investigation, Validation, Writing–review and editing. JR: Data curation, Methodology, Resources, Writing–review and editing. LS: Data curation, Formal Analysis, Methodology, Software, Validation, Writing–review and editing. BS: Data curation, Resources, Writing–review and editing. US: Data curation, Formal Analysis, Methodology, Validation, Writing–review and editing. PT-P: Data curation, Resources, Writing–review and editing. NT: Investigation,

Methodology, Validation, Writing–review and editing. MW: Conceptualization, Methodology, Resources, Writing–review and editing. PW: Data curation, Formal Analysis, Methodology, Resources, Software, Writing–review and editing.

Funding

The author(s) declare that financial support was received for the research, authorship, and/or publication of this article. This work has been financially supported by the German BMBF (project 05P21UMFN2), the Swedish Research Council (Vetenskapsrådet, VR 2016-3969), and the Knut and Alice Wallenberg Foundation (KAW 2015.0021). The publication is funded by the Open Access Publishing Fund of GSI Helmholtzzentrum für Schwerionenforschung.

Acknowledgments

The results presented here are based on the experiments U308 and U327, which were performed at the beam line X8/TASCA at the GSI Helmholtzzentrum für Schwerionenforschung GmbH, Darmstadt (Germany) in the frame of FAIR Phase-0. The authors would like to thank the GSI staff of the ECR ion source group and the accelerator UNILAC for providing stable and intense ion beams, as well as the GSI department of experiment electronics, and the detector and target laboratories of GSI. The ^{243}Am target material was provided by the U.S. DOE through ORNL.

Conflict of interest

The authors declare that the research was conducted in the absence of any commercial or financial relationships that could be construed as a potential conflict of interest.

Publisher's note

References

Aksenov, N. V., Steinegger, P., Abdullin, F.Sh., Albin, Yu. V., Bozhikov, G. A., Chepigin, V. I., et al. (2017). On the volatility of nihonium (Nh, Z = 113). *Eur. Phys. J.* A 53, 158. doi:10.1140/epja/i2017-12348-8

Becke, A. D. (1988). Density-functional exchange-energy approximation with correct asymptotic behavior. *Phys. Rev. A* 38, 3098–3100. doi:10.1103/physreva.38.3098

Borschevsky, A., Pašteka, L. F., Pershina, V., Eliav, E., and Kaldor, U. (2015). Ionization potentials and electron affinities of the superheavy elements 115–117 and their sixth-row homologues Bi, Po, and at. *Phys. Rev. A* 91, 020501. (R). doi:10.1103/physreva.91.020501

Brüchle, W. (2003). Confidence intervals for experiments with background and small numbers of events. *Radiochim. Acta* 91, 71–80. doi:10.1524/ract.91.2.71.19989

Desclaux, J. P. (1973). Relativistic Dirac-Fock expectation values for atoms with Z = 1 to Z = 120. *Data Nucl. Data Tables* 12, 311–406. doi:10.1016/0092-640x(73)90020-x

Dmitriev, S. N., Aksenov, N. V., Albin, Yu. V., Bozhikov, G. A., Chelnokov, M. L., Chepigin, V. I., et al. (2014). Pioneering experiments on the chemical properties of element 113. *Mendeleev Commun.* 24, 253–256. doi:10.1016/j.mencom.2014.09.001

Düllmann, Ch. E., Block, M., Heßberger, F. P., Khuyagbaatar, J., Kindler, B., Kratz, J. V., et al. (2022). Five decades of GSI superheavy element discoveries and chemical investigation. *Radiochim. Acta* 110 (6-9), 417–439. doi:10.1515/ract-2022-0015

Düllmann, Ch. E., Brüchle, W., Dressler, R., Eberhardt, K., Eichler, B., Eichler, R., et al. (2002). Chemical investigation of hassium (element 108). *Nature* 418, 859–862. doi:10.1038/nature00980

Düllmann, Ch. E., Folden, C. M., Gregorich, K. E., Hoffman, D. C., Leitner, D., Pang, G. K., et al. (2005). Heavy-ion-induced production and physical preseparation of short-lived isotopes for chemistry experiments. *Nucl. Instrum. Meth. A* 551, 528–539. doi:10.1016/j.nima.2005.05.077

Düllmann, Ch. E., Schädel, M., Yakushev, A., Türler, A., Eberhardt, K., Kratz, J. V., et al. (2010). Production and decay of element 114: high cross sections and the new nucleus ^{277}Hs. *Phys. Rev. Lett.* 104, 252701. doi:10.1103/physrevlett.104.252701

Dzuba, V. A., and Flambaum, V. V. (2016). Electron structure of superheavy elements uut, Fl and uup (Z=113 to 115). *Hyperfine Interact.* 237, 160. doi:10.1007/s10751-016-1365-7

Eichler, R. (2013). First foot prints of chemistry on the shore of the Island of Superheavy Elements. *J. Phys. Conf. Ser.* 420, 012003. doi:10.1088/1742-6596/420/1/012003

Eichler, R., Aksenov, N. V., Albin, Yu. V., Belozerov, A. V., Bozhikov, G. A., Chepigin, V. I., et al. (2010). Indication for a volatile element 114. *Radiochim. Acta* 98, 133–139. doi:10.1524/ract.2010.1705

Eichler, R., Aksenov, N. V., Belozerov, A. V., Bozhikov, G. A., Chepigin, V. I., Dmitriev, S. N., et al. (2007). Chemical characterization of element 112. *Nature* 447, 72–75. doi:10.1038/nature05761

Eliav, E., Fritzsche, S., and Kaldor, U. (2015). Electronic structure theory of the superheavy elements. *Nucl. Phys. A* 944, 518–550. doi:10.1016/j.nuclphysa.2015.06.017

Forsberg, U., Rudolph, D., Andersson, L.-L., Di Nitto, A., Düllmann, Ch. E., Fahlander, C., et al. (2016). Recoil-α-fission and recoil-α–α-fission events observed in the reaction ^{48}Ca + ^{243}Am. *Nucl. Phys. A* 953, 117–138. doi:10.1016/j.nuclphysa.2016.04.025

Fox-Beyer, B. S., and van Wüllen, C. (2012). Theoretical modelling of the adsorption of thallium and element 113 atoms on gold using two-component density functional methods with effective core potentials. *Chem. Phys.* 395, 95–103. doi:10.1016/j.chemphys.2011.04.029

Frenkel, Ya. I. (1948). *Statistical physics*. Moscow-Leningrad: Izd. Akad. Nauk SSSR. [book in Russian].

Gates, J. M., Gregorich, K. E., Gothe, O. R., Uribe, E. C., Pang, G. K., Bleuel, D. L., et al. (2015). Decay spectroscopy of element 115 daughters: ^{280}Rg → ^{276}Mt and ^{276}Mt → ^{272}Bh. *Phys. Rev. C* 92, 021301. (R). doi:10.1103/physrevc.92.021301

Götz, S., Raeder, S., Block, M., Düllmann, Ch. E., Folden III, C. M., Glennon, K. J., et al. (2021). Rapid extraction of short-lived isotopes from a buffer gas cell for use in gas-phase chemistry experiments, Part II: on-line studies with short-lived accelerator-produced radionuclides. *B* 507, 27–35. doi:10.1016/j.nimb.2021.09.004

Hohenberg, P., and Kohn, W. (1964). Inhomogeneous electron gas. *Phys. Rev. B* 136, 864–B871. doi:10.1103/physrev.136.b864

Ilias, M., and Pershina, V. (2022). Reactivity of group 13 elements Tl and element 113, Nh, and of their hydroxides with respect to various quartz surfaces from periodic relativistic DFT calculations. *Inorg. Chem.* 61 (40), 15910–15920. doi:10.1021/acs.inorgchem.2c02103

Jäger, E., Brand, H., Düllmann, Ch.E., Khuyagbaatar, J., Krier, J., Schädel, M., et al. (2014). High intensity target wheel at TASCA: target wheel control system and target monitoring. *J. Radioanal. Nucl. Chem.* 299, 1073–1079. doi:10.1007/s10967-013-2645-1

Khuyagbaatar, J., Ackermann, D., Andersson, L.-L., Ballof, J., Brüchle, W., Düllmann, Ch. E., et al. (2012). Study of the average charge states of ^{188}Pb and ^{252,254}No ions at the gas-filled separator TASCA. *Nucl. Instr. Meth. A* 689, 40–46. doi:10.1016/j.nima.2012.06.007

Kohn, W., and Sham, L. J. (1965). Self-consistent equations including exchange and correlation effects. *Phys. Rev. A* 140, 1133–A1138. doi:10.1103/physrev.140.a1133

Kraus, B. (2021). *Optimization of vacuum adsorption chromatography for superheavy element experiments [Doctoral dissertation]*. Switzerland: University of Bern.

Lens, L., Yakushev, A., Düllmann, Ch. E., Asai, M., Ballof, J., Block, M., et al. (2018). Online chemical adsorption studies of Hg, Tl, and Pb on SiO_2 and Au surfaces in preparation for chemical investigations on Cn, Nh, and Fl at TASCA. *Radiochim. Acta* 106, 949–962. doi:10.1515/ract-2017-2914

Oganessian, Yu Ts., Abdullin, F.Sh., Dmitriev, S. N., Gostic, J. M., Hamilton, J. H., Henderson, R. A., et al. (2013). Investigation of the ^{243}Am + ^{48}Ca reaction products previously observed in the experiments on elements 113, 115, and 117. *Phys. Rev. C* 87, 014302. doi:10.1103/physrevc.87.014302

Oganessian, Yu. Ts., and Utyonkov, V. K. (2015). Superheavy nuclei from ^{48}Ca-induced reactions. *Nucl. Phys. A* 944, 62–98. doi:10.1016/j.nuclphysa.2015.07.003

Oganessian, Yu. Ts., Utyonkov, V. K., Kovrizhnykh, N. D., Abdullin, F.Sh., Dmitriev, S. N., Dzhioev, A. A., et al. (2022). New isotope ^{286}Mc produced in the ^{243}Am + ^{48}Ca reaction. *Phys. Rev. C* 106, 064306. doi:10.1103/physrevc.106.064306

Oganessian, Yu. Ts., Utyonkov, V. K., Kovrizhnykh, N. D., Abdullin, F.Sh., Dmitriev, S. N., Ibadullayev, D., et al. (2022). First experiment at the Super Heavy Element Factory: high cross section of ^{288}Mc in the ^{243}Am + ^{48}Ca reaction and identification of the new isotope ^{264}Lr. *Phys. Rev. C* 106, L031301. doi:10.1103/PhysRevC.106.L031301

Pershina, V. (2015). Electronic structure and properties of superheavy elements. *Nucl. Phys. A* 944, 578–613. doi:10.1016/j.nuclphysa.2015.04.007

Pershina, V. (2016). A theoretical study on the adsorption behavior of element 113 and its homologue Tl on a quartz surface: relativistic periodic DFT calculations. *J. Phys. Chem. C* 120 (36), 20232–20238. doi:10.1021/acs.jpcc.6b07834

Pershina, V. (2018). Reactivity of superheavy elements Cn, Nh, and Fl and their lighter homologues Hg, Tl, and Pb, respectively, with a gold surface from periodic DFT calculations. *Inorg. Chem.* 57 (7), 3948–3955. doi:10.1021/acs.inorgchem.8b00101

Pershina, V. (2019). Relativity in the electronic structure of the heaviest elements and its influence on periodicities in properties. *Radiochim. Acta* 107, 833–863. doi:10.1515/ract-2018-3098

Pershina, V., Anton, J., and Jacob, T. (2009). Electronic structures and properties of M-Au and MOH, where M = Tl and element 113. *Chem. Phys. Lett.* 480, 157–160. doi:10.1016/j.cplett.2009.08.069

Pershina, V., and Iliaš, M. (2019). Properties and reactivity of hydroxides of group 13 elements in, Tl, and Nh from molecular and periodic DFT calculations. *Inorg. Chem.* 58, 9866–9873. doi:10.1021/acs.inorgchem.9b00949

Pershina, V., Ilias, M., and Yakushev, A. (2021). Reactivity of the superheavy element 115, Mc, and its lighter homologue, Bi, with respect to gold and hydroxylated quartz surfaces from periodic relativistic DFT calculations: a comparison with element 113. *Nh. Inorg. Chem.* 60 (13), 9848–9856.

Pitzer, K. S. (1975). Are elements 112, 114, and 118 relatively inert gases? *J. Chem. Phys.* 63, 1032–1033. doi:10.1063/1.431398

Pyper, N. C. (2020). Relativity and the periodic table. *Phil. Trans. R. Soc. A* 378, 20190305. doi:10.1098/rsta.2019.0305

Rudolph, D. (2022). Results and plans for nuclear spectroscopy of superheavy nuclei: the Lund perspective. *Eur. Phys. J.* A 58, 242. doi:10.1140/epja/s10050-022-00868-7

Rudolph, D., Forsberg, U., Golubev, P., Sarmiento, L. G., Yakushev, A., Andersson, L.-L., et al. (2013). Spectroscopy of element 115 decay chains. *Phys. Rev. Lett.* 111, 112502. doi:10.1103/physrevlett.111.112502

Runke, J., Düllmann, Ch. E., Eberhardt, K., Ellison, P. A., Gregorich, K. E., Hofmann, S., et al. (2014). Preparation of actinide targets for the synthesis of the heaviest elements. *J. Radioanal. Nucl. Chem.* 299, 1081–1084. doi:10.1007/s10967-013-2616-6

Rusakov, A. A., Demidov, Y. A., and Zaitsevskii, A. (2013). Estimating the adsorption energy of element 113 on a gold surface. *Centr. Eur. J. Phys.* 11, 1537–1540. doi:10.2478/s11534-013-0311-4

Såmark-Roth, A., Cox, D. M., Rudolph, D., Sarmiento, L. G., Albertsson, M., Carlsson, B. G., et al. (2023). Spectroscopy along flerovium decay chains. III. details on experiment, analysis, ^{282}Cn, and spontaneous fission branches. *Phys. Rev. C* 107, 024301. doi:10.1103/PhysRevC.107.024301

Schwerdtfeger, P., and Seth, M. (2002). Relativistic quantum chemistry of the superheavy elements. Closed-shell element 114 as a case study. *J. Nucl. Radiochem. Sci.* 3 (1), 133–136. doi:10.14494/jnrs2000.3.133

Schwerdtfeger, P., Smits, O. R., and Pyykkö, P. (2020). The periodic table and the physics that drives it. *Nat. Rev. Chem.* 4, 359–380. doi:10.1038/s41570-020-0195-y

SCM (2024). *Amsterdam modelling suite AMS ADF 2024.1, SCM, theoretical chemistry*. Amsterdam, Netherlands: Vrije Universiteit. Available at: http://www.scm.com.

Semchenkov, A., Brüchle, W., Jäger, E., Schimpf, E., Schädel, M., Mühle, C., et al. (2008). The TransActinide separator and chemistry apparatus (TASCA) at GSI – optimization of ion-optical structures and magnet designs. *Nucl. Instrum. Methods B* 266, 4153–4161. doi:10.1016/j.nimb.2008.05.132

Serov, A., Eichler, R., Dressler, R., Piguet, D., Türler, A., Vögele, A., et al. (2013). Adsorption interaction of carrier-free thallium species with gold and quartz surfaces. *Radiochim. Acta* 101, 421–426. doi:10.1524/ract.2013.2045

Steinegger, P., Asai, M., Dressler, R., Eichler, R., Kaneya, Y., Mitsukai, A., et al. (2016). Vacuum chromatography of Tl on SiO_2 at the single-atom level. *J. Phys. Chem. C* 120, 7122–7132. doi:10.1021/acs.jpcc.5b12033

Smits, O. R., Düllmann, Ch. E., Indelicato, P., Nazarewicz, W., and Schwerdtfeger, P. (2024). The quest for superheavy elements and the limit of the periodic table. *Nat. Rev. Phys.* 6, 86–98. doi:10.1038/s42254-023-00668-y

Te Velde, G., Bickelhaupt, F. M., Baerends, E. J., Fonseca Guerra, C., Van Gisbergen, S. J. A., Snijders, J. G., et al. (2001). Chemistry with ADF. *J. Comput. Chem.* 22 (9), 931–967. doi:10.1002/jcc.1056

Trombach, L., Ehlert, S., Grimme, S., Schwerdtfeger, P., and Mewes, J.-M. (2019). Exploring the chemical nature of super-heavy main-group elements by means of efficient plane-wave density-functional theory. *Phys. Chem. Chem. Phys.* 21 (33), 18048–18058. doi:10.1039/c9cp02455g

Türler, A., Eichler, R., and Yakushev, A. (2015). Chemical studies of elements with Z ≥ 104 in gas phase. *Nucl. Phys. A* 944, 640–689. doi:10.1016/j.nuclphysa.2015.09.012

Türler, A., and Pershina, V. (2013). Advances in the production and chemistry of the heaviest elements. *Chem. Rev.* 113 (2), 1237–1312. doi:10.1021/cr3002438

Van Lenthe, E., Baerends, E. J., and Snijders, J. G. (1994). Relativistic total energy using regular approximations. *J. Chem. Phys.* 101, 9783–9792. doi:10.1063/1.467943

Varentsov, V., and Yakushev, A. (2019). Concept of a new universal high-density gas stopping cell setup for study of gas-phase chemistry and nuclear properties of super heavy elements (UniCell). *Nucl. Instrum. Methods A* 940, 206–214. doi:10.1016/j.nima.2019.06.032

Węgrzecki, M., Bar, J., Budzyński, T., Cież, M., Grabiec, P., Kozłowski, R., et al. (2013). "Design and properties of silicon charged-particle detectors developed at the Institute of electron technology (ITE)," in Proc. SPIE 8902, Electron Technology Conference 2013, China, 25 July 2013. doi:10.1117/12.2031041

Wittwer, D., Abdullin, F.Sh., Aksenov, N. V., Albin, Yu. V., Bozhikov, G. A., Dmitriev, S. N., et al. (2010). Gas phase chemical studies of superheavy elements using the Dubna gas-filled recoil separator - stopping range determination. *Nucl. Instr. Meth. B* 268, 28–35. doi:10.1016/j.nimb.2009.09.062

Yakushev, A., and Eichler, R. (2016). Gas-phase chemistry of element 114, flerovium. *EPJ Web Conf.* 131, 07003. doi:10.1051/epjconf/201613107003

Yakushev, A., Gates, J. M., Türler, A., Schädel, M., Düllmann, Ch. E., Ackermann, D., et al. (2014). Superheavy element Flerovium (element 114) is a volatile metal. *Inorg. Chem.* 53, 1624–1629. doi:10.1021/ic4026766

Yakushev, A., Lens, L., Düllmann, Ch. E., Block, M., Brand, H., Dasgupta, M., et al. (2021). First study on nihonium (Nh, element 113) chemistry at TASCA. *Front. Chem.* 9, 753738. doi:10.3389/fchem.2021.753738

Yakushev, A., Lens, L., Düllmann, Ch. E., Khuyagbaatar, J., Jäger, E., Krier, J., et al. (2022). On the adsorption and reactivity of element 114, flerovium. *Front. Chem.* 10, 976635. doi:10.3389/fchem.2022.976635

Zhang, Y., Evans, J. R. G., and Yang, S. (2011). Corrected values for boiling points and enthalpies of vaporization of elements in handbooks. *J. Chem. Eng. Data* 56, 328–337. doi:10.1021/je1011086

Zvára, I. (1985). Simulation of thermochromatographic processes by the Monte Carlo method. *Radiochim. Acta* 38, 95–102. doi:10.1524/ract.1985.38.2.95